Integrating fMRI-based pain signatures into a broader neuroscience context

Gabriel Riegner & Kevin Nguyen

Scientific background

The experience of pain is multidimensional and constructed through a combination of sensory inputs, expectations, memories, and other context information. Coordinating such an experience is the central nervous system, from sensory neurons that send information to the spinal cord and brainstem, to regions of the brain and cortex which process more abstract dimensions of pain. Because of this complexity, pain cannot be localized to one brain region, say the insula, but instead relies on pathways that connect the insula to other regions. This results in a cross-talk between distributed brain regions, systems, and networks.

Mapping this pattern of neural responses to pain can be achieved by functional magnetic brain imaging (fMRI) and modeling approaches capable of summarizing the resulting high dimensional spatial data. An example of this comes from (Woo et al. 2017)*, "Quantifying cerebral contributions to pain beyond nociception."* Here, the authors used machine learning to develop a multivariate pattern biomarker–termed the stimulus intensity independent pain signature (SIIPS)–that accurately predicts trial-by-trial pain ratings independent of the stimulus intensity. The sensitivity and specificity of this biomarker was demonstrated in the paper through cross-validation in four fMRI training datasets and two independent test sets. The SIIPS pattern shows activity in lateral prefrontal cortex and parahippocampal cortices, nucleus accumbens, and other brain regions involved in pain processing. This brain map, registered to a standard coordinate space, is the outcome variable of our multiple regression analysis.

Objectives

The research question we are trying to answer is how this spatial pattern of pain-evoked activation fits into the broader context of brain organization by bridging types of neural data. Over the past decade in neuroscience, researchers have measured the human brain with increasing spatial and temporal resolution–using imaging, recording, tracing and sequencing technologies. This has allowed for depth in understanding the structure and function of the brain, including its myelination, gray matter morphometry, gene expression, cytoarchitecture, metabolism, intrinsic dynamics, and other measures. A curated library of more than 40 of these brain maps has been collected into a software tool, *Neuromaps* (Markello et al. 2022). This open-access resource allows us to contextualize the pain signature (SIIPS) map with respect to existing structural and functional annotations. In the context of multiple regression, we will statistically compare the spatial topographies of the SIIPS to a linear combination of Neuromaps predictors to identify map-to-map similarities.

Data description

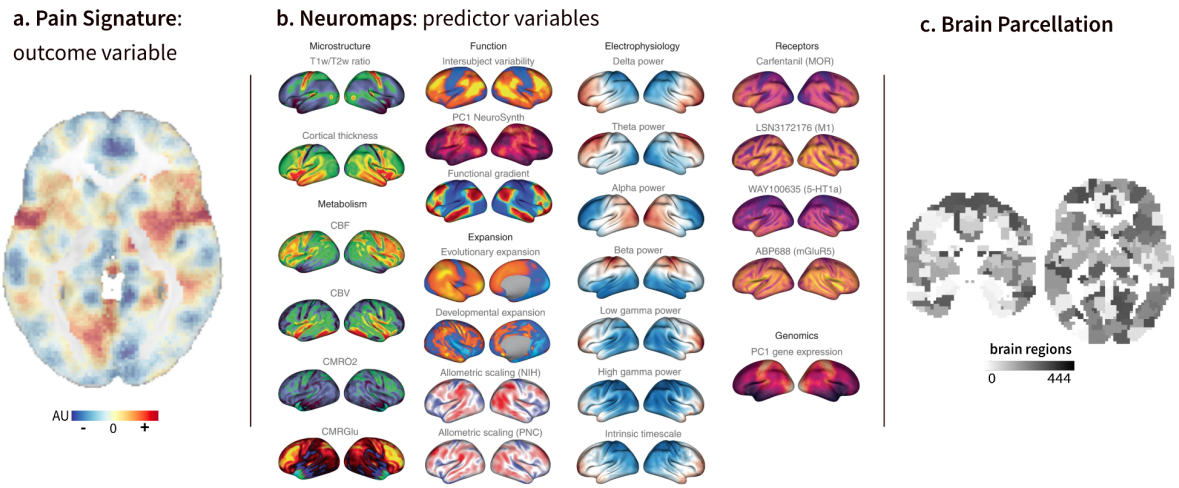

A: **Pain Signature.** The stimulus intensity independent pain signature, described by Woo et al., 2017, is a measure of pain evoked activation. The image shows prediction weights in arbitrary units (A.U.). Regional averages based on the 444-region parcellation in (c) were extracted to represent the outcome variable as a column vector.

B: **Neuromaps.** A representative subset of the Neuromaps images (Markello et al., 2022) were used as predictors in the regression model. We only considered brain maps that had whole brain coverage (including sub-cortex and cortex), as most regions important for pain processing are located below the cortical surface. All maps were spatially transformed into the same coordinate space before regional averages were extracted using the parcelation in (c). This allowed us to create an initial design matrix that included 34 columns vectors for each map, with rows representing each of the 444 brain regions.

These 34 brain maps represent various functions of the brain, as well as the physiological processes that underlie these functions. The images can be divided into four main categories: cognitive activation, cerebral blood flow, synaptic density, and neurotransmitter densities. Each category incorporates data from different publications and imaging modalities, including (functional) magnetic resonance imaging, arterial spin labeling, and positron emission tomography.

The cognitive activation map comes from the Neurosynth meta-analysis platform for neuroimaging and represents the principal component direction of brain activations elicited across hundreds of cognitive experiments (Yarkoni and Westfall 2017). Cerebral blood flow describes the perfusion of blood through arteries in the brain, and the rate of flow to different regions (Satterthwaite et al. 2014). The synaptic density map approximates the number of neuron-to-neuron connections across the brain, which indicate where densities of neurotransmitters are located in the brain (Finnema et al. 2016). Lastly, individual classes of neurotransmitters have been imaged using PET and molecule-specific radiotracers. In our analyses we used maps of neurotransmitter densities for endogenous opioids (Kantonen et al. 2020; Turtonen et al. 2021), dopamine (Dukart et al. 2018; Jaworska et al. 2020; Sandiego et al. 2015; Kaller et al. 2017; Sasaki et al. 2012; Smith et al. 2017), serotonin (Fazio et al. 2016; Gallezot et al. 2010; Radhakrishnan et al. 2018), acetylcholine (Aghourian et al. 2017; Bedard et al. 2019; Hillmer et al. 2016; Naganawa et al. 2021), glutamate (DuBois et al. 2015), GABA (Dukart et al. 2018), cannabinoids (Laurikainen et al. 2019; Normandin et al. 2015), norepinephrine (Gallezot et al. 2011), and histamine (Gallezot et al. 2017).

c: **Brain parcellation.** Deterministic brain parcellation of 444 regions generated from a group of 200 subjects (Bellec et al. 2010).

Data preprocessing and variable selection

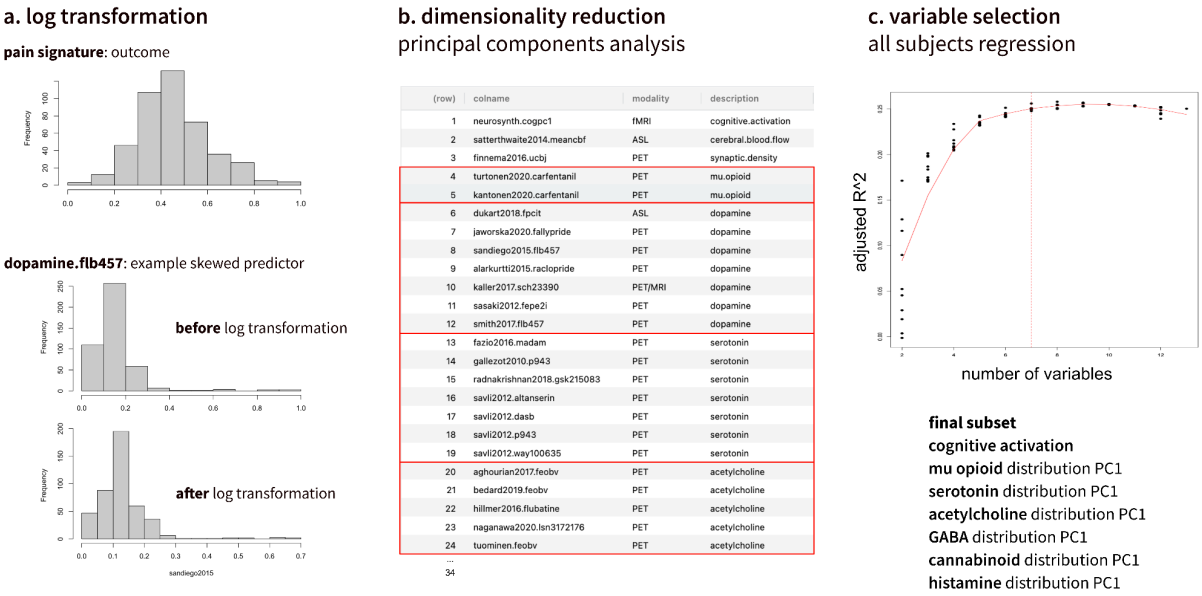

a: Variable distribution plot. From the predictors, a histogram of each was plotted to identify those with skewed distributions that were then log transformed. Because some of the predictors had negative values, and the majority had arbitrary units, we normalized them to a range of 0-1 through the function $\frac{x-min(x)}{max(x)-min(x)}$. This was also done to make the logarithmic transformation possible. Plotted here is an example where the log of the predictor, *dopamine.flb457*, helped reduce its skew. The distribution of the response variable, on the other hand, is approximately Gaussian.

b: Dimensionality reduction. The 34 initial predictors can be grouped into 12 categories based on similarities between brain maps. These categories include cognitive activation, cerebral blood flow, synaptic density, and nine neurotransmitter subtypes. To reduce the set of explanatory variables in our model, we grouped each neurotransmitter subtype into a lower dimensional space using principal component analysis. For instance, the variables *turtonen2020.carfentanil* and *kantonen2020.carfentanil* both measure the density of opioid receptors and were grouped together. We selected the first component of each category which represented the most variability across brain maps. This allowed us to reduce the number of predictors to 12 without losing important information about the distribution of each neurotransmitter throughout the brain.

c: Variable selection. To further reduce the number of predictors, we used an all subsets regression approach to find the combination of predictor variables that results in the maximum adjusted R-squared value (*Subset Selection in Regression* 2002). This method of variable selection considers all possible combinations of predictor variables (2^12), allowing us to identify the combination that results in the best model fit. The graph shows that increasing the number of variables in the multiple regression model increases the variance explained in the pain signature map, while increasing past seven predictors gives the model no additional explanatory power. The final subset includes the seven predictor variables that

explain the most variance in the pain signature, while accounting for the number of predictors in the model.

Qualitative description

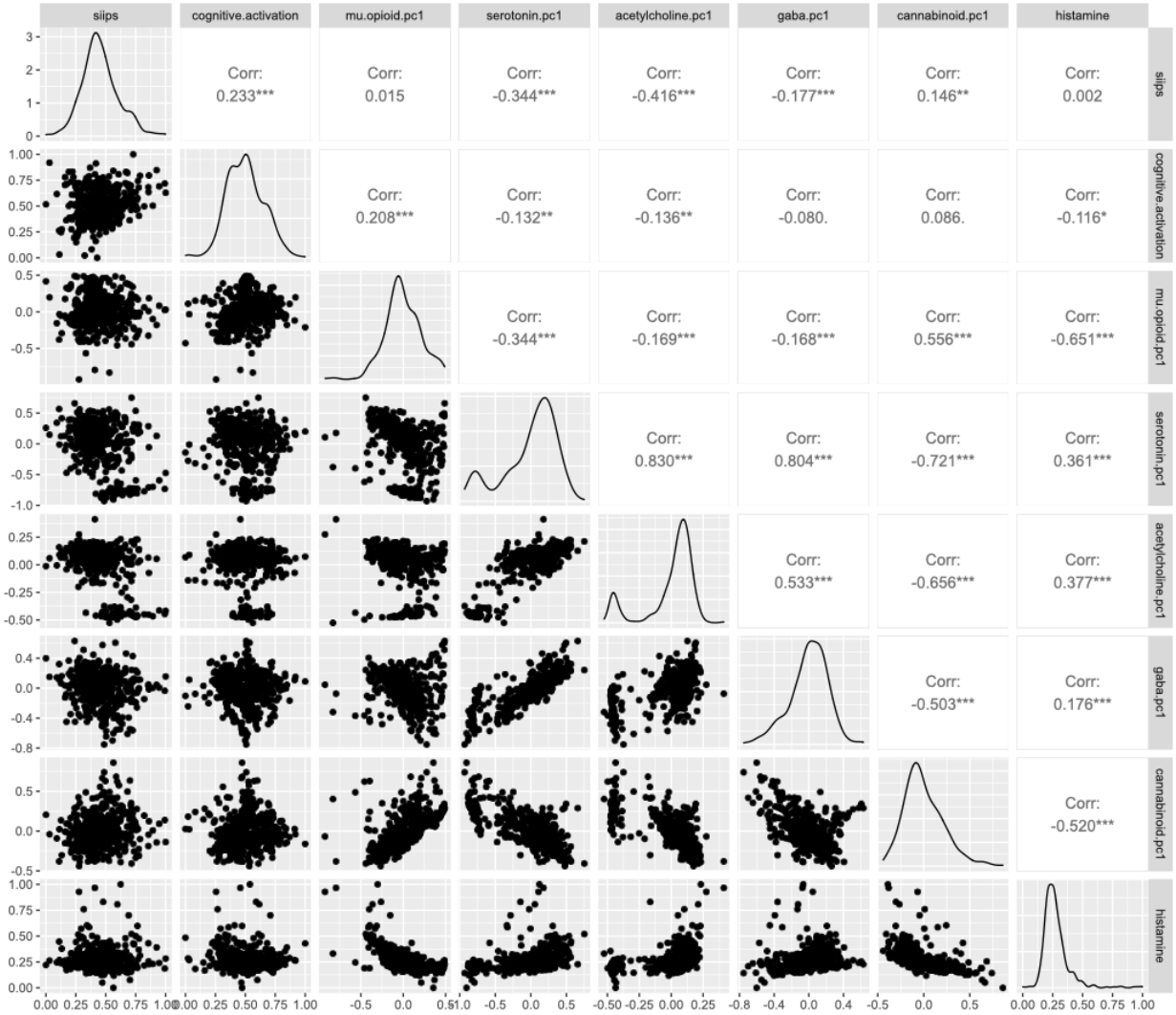

a: Pairs plot. A total of seven predictors from the variable selection stage were plotted against the pain signature (SIIPS) response variable. In a few of the graphs, the data seems to be normally distributed whereas some other variables such as *serotonin.pc1* and *acetylcholine.pc1* are observed to have a bimodal distribution. This is especially notable in the graphs where there are two clusters of data points, one for each peak. In other instances, the plots display nonlinearities within the data such as in the plot graphing *mu.opioid.pc1* and *histamine* which shows an exponential trend. Collinearity is also a problem within the predictors as many of them, such as *serotonin.pc1* and *gaba.pc1*, have a high degree of correlation with each other.

Naive model and diagnostics

The naive model is an OLS regression of the response variables (SIIPS) as a function of each of the seven predictors above, with no higher order terms.

a. residual plots

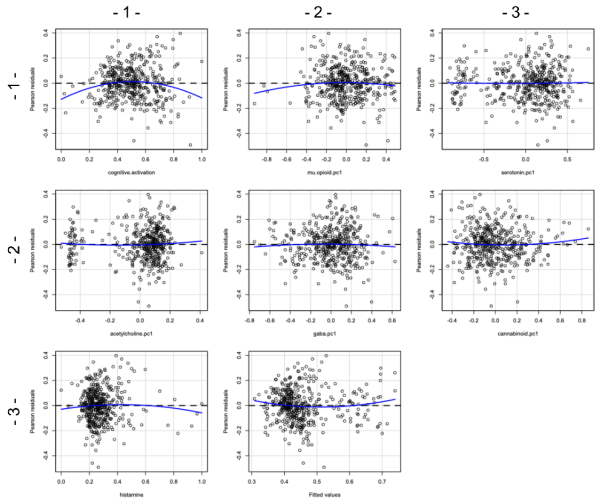

b. nonlinearity

(row)	Test stat	Pr(>|Test stat|)
cognitive.activation	-3.0341	0.0026
mu.opioid.pc1	-1.6227	0.1054
serotonin.pc1	0.2382	0.8119
acetylcholine.pc1	0.7013	0.4835
gaba.pc1	-0.6238	0.5331
cannabinoid.pc1	1.084	0.279
histamine	-1.1978	0.2317
Tukey test	1.9282	0.0538

c. collinearity

vif(ols1)
1.0884
2.8384
10.4786
5.3587
3.7836
3.0159
2.1033

d. heteroscedasticity

```
Non-constant Variance Score Test
Variance formula: ~ fitted.values
Chisquare = 8.132561, Df = 1, p = 0.0043477
```

e. autocorrelation

```
 lag Autocorrelation D-W Statistic p-value
   1      0.01911599      1.961691     0.7
Alternative hypothesis: rho != 0
```

a: Residual plots. The residual errors in the naive model were plotted against each regressor in the model, as well as against the fitted values. From these plots we identified non-linearity between the pain signature maps and the regressors for *cognitive activation* (row 1, col 1) and *mu opioids* (row 1, col 2). The downward bending blue curve indicates that there is an approximate quadratic relationship between these predictors and the response. This was confirmed by a formal test for nonadditivity in (b).

The residual plots also indicate a problem of non-constant variance, which we confirmed in a formal test for heteroscedasticity (d). For instance, the residuals in relation to *serotonin* (row 1, col 3) and *acetylcholine* (row 2, col 1) show a bimodal distribution. This suggests that these neurotransmitters are not evenly distributed across the brain and tend to cluster in different regions. Since this is likely an important characteristic of the data, we decided not to alter their distributions and instead bootstrapped estimates for variance in the next models.

b: Tukey test for nonadditivity. This statistical test is used to determine whether quadratic terms should be included in the regression model if they are significantly different from zero (Weisberg 2014). From this test we decided to add quadratic terms for the cognitive activation ($p = 0.003$) and mu opioid ($p = 0.1$) predictors in the next iteration of the model.

c: Collinearity. From the pairs plot above, there is evident correlation between some of the predictors: *serotonin-GABA*, *serotonin-acetylcholine*, etc. Highly correlated predictors are a problem for model estimation. The variance inflation factor (VIF) of a predictor measures the degree to which it is correlated with other predictors in the model, and a VIF above five generally indicates a large inflation of the variance estimates (Fox and Monette 1992). Because of this, *serotonin* with a VIF of 10.48 was removed as a predictor as much of its variability can be explained by acetylcholine alone.

d: Heteroscedasticity. A formal test of heteroscedasticity, the score test for non-constant variance, indicates that we should reject the hypothesis of constant variance for the residuals (Weisberg 2014).

e: Autocorrelation. Since we are working with brain maps that are spatially autocorrelated, i.e. the observation units are not independent, there is likely to be autocorrelation in the residuals which would

violate the assumption of independence of the OLS regression model. We tested the degree of correlation between the residual and lagged version of the residuals, using the Durbin-Watson statistic (Weisberg 2014). The correlation coefficient (0.02) was not statistically significant, so we cannot claim that the residuals are autocorrelated. We conclude that the degree of spatial autocorrelation is not biasing our OLS parameter estimates.

Final model and diagnostics

The final model aimed to address the problems of nonlinearity, collinearity, and heteroscedasticity evident in the naive model. An update to the OLS model removed *serotonin* as a predictor and added quadratic terms for *cognitive activation* and *mu opioids*. An ANOVA test of the naive model versus the final model indicates that the updated model fits the data better (*F=8.2, p = 0.004*).

a. residual plots

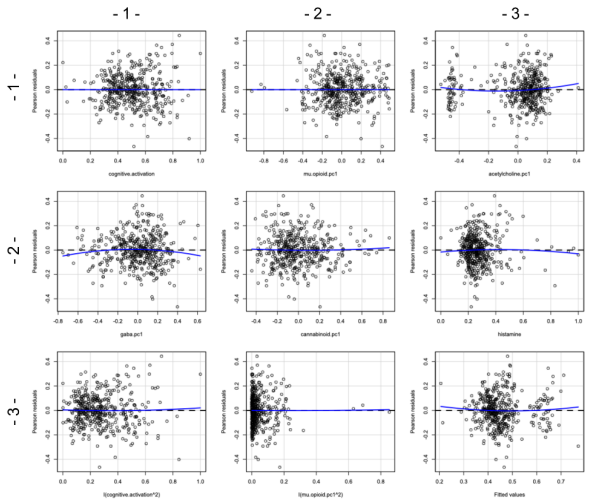

b. diagnostics

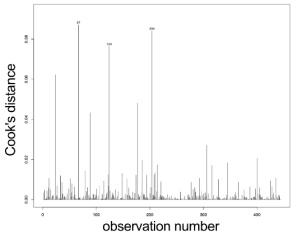

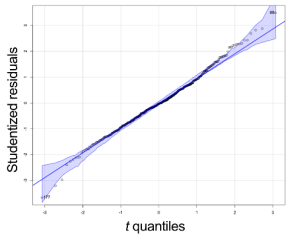

c. model summary

(row)	Estimate	Std.Error	t.value	p.value	2.5%	97.5%
(Intercept)	0.119	0.064	1.855	0.064	-0.015	0.238
cognitive.activation	0.795	0.25	3.18	0.002	0.348	1.315
mu.opioid.pc1	0.093	0.049	1.903	0.058	0.004	0.19
acetylcholine.pc1	-0.469	0.056	-8.332	0	-0.57	-0.355
gaba.pc1	0.045	0.037	1.206	0.228	-0.032	0.12
cannabinoid.pc1	-0.09	0.055	-1.632	0.103	-0.201	0.018
histamine	0.42	0.1	4.203	0	0.244	0.647
I(cognitive.activation^2)	-0.616	0.259	-2.38	0.018	-1.124	-0.143
I(mu.opioid.pc1^2)	-0.205	0.087	-2.348	0.019	-0.384	-0.05

a: Residual plots. The residual plots show individual predictors and fitted values of the final model plotted against the Pearson residuals. All of the predictors now show a linear relationship with the residuals, including *cognitive activation* (row 1, col 1) and *mu opioids* (row 1, col 2). A Tukey test for non-additivity that confirms adding quadratic terms for these variables fixes the non-linearities (*ps > 0.05*).

Also evident in the residual plots is the previously discussed non-constant variance (*p = 0.005*). Because of this, we disregarded the OLS standard errors and recomputed these estimates, and the statistics that depend on them, using nonparametric bootstrap. We ran 1000 bootstrap iterations, and for each update, resampled with replacement all 444 observations. For each iteration, we extracted the coefficients using the formula of the final model, and calculated the standard errors under heteroscedasticity as the standard deviations of these estimates. *T*-statistics were then computed by dividing the original OLS coefficients by the bootstrap estimates of standard errors. *P*-values were calculated by 2*Pr(-|*t-statistic*|) given (444 - 8 = 436) degrees of freedom. Additionally, we used the distribution of bootstrap coefficients to estimate the 95% confidence intervals for each coefficient. All the values are summaries in table (c).

b: Diagnostics. Taking a look at the diagnostics, we see that there are three points that seem to exert the most influence on the entire model: 67, 124, and 204 based on Cook's distance. Likewise, the studentized residuals have an approximate *t*-distribution.

c: Model summary. In this study, we were able to say that the final model with the 6 predictors (8 regressors) accounted for 27% of the variability within the pain signature. The significant regressors from the model included *cognitive activation* (0.80, $p = 0.002$), *acetylcholine* (-0.47, $p = 0$), *histamine* (0.42, $p = 0$), *I(cognitive activation^2)* (-0.62, $p = 0.018$), and *I(mu opioid^2)* (-0.21, $p = 0.02$). Only the *cognitive activation* and *histamine* regressors were positive whereas the other regressors all displayed a negative coefficient. Further work and research will need to be done and looked into this to see if these findings make sense despite their statistical significance. The nonsignificant predictors include *mu opioid* (0.09, $p = 0.057$), *gaba* (0.05, $p = 0.23$), *cannabinoid* (-0.09, $p = 0.089$), and likely all of the other predictors that we removed previously such as *serotonin* and the ones omitted from the all subsets regression.

Conclusion

In reference to the initial goal of explaining the distributed pattern of brain activation that relates to the experience of pain, we have narrowed down a set of spatial maps of brain function and physiology that explain over a quarter of its region-to-region variance. To improve prediction and variance explained, more research, data gathering, and analysis would need to be completed. For what we have in the model summary, many of the significant predictors of pain make sense in the broader scientific context. For example, *cognitive activation* shows a significant positive association with the pain signature, meaning their spatial maps are relatively homogeneous while controlling for the other predictors. This makes sense in context because the experience of pain is constructed through the interaction of sensory, emotional, and cognitive networks and brain regions. Likewise, *mu opioids* are important neurotransmitters for the endogenous modulation of pain, and are located most densely in brainstem regions that process ascending pain inputs. The other significant predictors, *acetylcholine* and *histamine*, have not been studied much in the context of pain research, but could be avenues for further exploration.

Contributions

Gabriel: Scientific background, Objectives, Data description, Data preprocessing and variable selection, Qualitative description, Naive model and diagnostics, Final model and diagnostics, Conclusions, Code
Kevin: Data description, Data preprocessing and variable selection, Qualitative description, Naive model and diagnostics, Final model and diagnostics, Conclusion, Code

Citations

Aghourian, Meghmik, C Legault-Denis, Jean-Paul Soucy, Pedro Rosa, S Gauthier, Alexey Kostikov, P Gravel, and Marc-Andre Bedard. 2017. “Quantification of Brain Cholinergic Denervation in Alzheimer’s Disease Using PET Imaging with [18F]-FEOBV.” *Molecular Psychiatry* 22 (September). https://doi.org/10.1038/mp.2017.183.

Bedard, Marc-Andre, Meghmik Aghourian, Camille Legault-Denis, Ronald B. Postuma, Jean-Paul Soucy, Jean-François Gagnon, Amélie Pelletier, and Jacques Montplaisir. 2019. “Brain Cholinergic Alterations in Idiopathic REM Sleep Behaviour Disorder: A PET Imaging Study with 18F-FEOBV.” *Sleep Medicine* 58 (June): 35–41. https://doi.org/10.1016/j.sleep.2018.12.020.

Bellec, Pierre, Pedro Rosa-Neto, Oliver C. Lyttelton, Habib Benali, and Alan C. Evans. 2010. “Multi-Level Bootstrap Analysis of Stable Clusters in Resting-State FMRI.” *NeuroImage* 51 (3): 1126–39. https://doi.org/10.1016/j.neuroimage.2010.02.082.

DuBois, Jonathan, Olivier Rousset, Jared Rowley, Manuel Porras-Betancourt, Andrew Reader, Aurelie Labbe, Gassan Massarweh, Jean-Paul Soucy, Pedro Rosa, and Eliane Kobayashi. 2015. “Characterization of Age/Sex and the Regional Distribution of MGluR5 Availability in the Healthy Human Brain Measured by High-Resolution [C]ABP688 PET.” *Eur J Nucl Med Mol Imaging*, August. https://doi.org/10.1007/s00259-015-3167-6.

Dukart, Juergen, Štefan Holiga, Christopher Chatham, Peter Hawkins, Anna Forsyth, Rebecca McMillan, Jim Myers, et al. 2018. “Cerebral Blood Flow Predicts Differential Neurotransmitter Activity.” *Scientific Reports* 8 (1): 4074. https://doi.org/10.1038/s41598-018-22444-0.

Fazio, P., M. Schain, K. Varnäs, C. Halldin, L. Farde, and A. Varrone. 2016. “Mapping the Distribution of

Serotonin Transporter in the Human Brainstem with High-Resolution PET: Validation Using Postmortem Autoradiography Data." *NeuroImage* 133 (June): 313–20. https://doi.org/10.1016/j.neuroimage.2016.03.019.

Finnema, Sjoerd J., Nabeel B. Nabulsi, Tore Eid, Kamil Detyniecki, Shu-fei Lin, Ming-Kai Chen, Roni Dhaher, et al. 2016. "Imaging Synaptic Density in the Living Human Brain." *Science Translational Medicine* 8 (348). https://doi.org/10.1126/scitranslmed.aaf6667.

Fox, John, and Georges Monette. 1992. "Generalized Collinearity Diagnostics." *Journal of the American Statistical Association* 87 (417): 178–83. https://doi.org/10.1080/01621459.1992.10475190.

Gallezot, Jean-Dominique, Nabeel Nabulsi, Alexander Neumeister, Beata Planeta-Wilson, Wendol A Williams, Tarun Singhal, Sunhee Kim, et al. 2010. "Kinetic Modeling of the Serotonin 5-HT1B Receptor Radioligand [11C]P943 in Humans." *Journal of Cerebral Blood Flow & Metabolism* 30 (1): 196–210. https://doi.org/10.1038/jcbfm.2009.195.

Gallezot, Jean-Dominique, Beata Planeta, Nabeel Nabulsi, Donna Palumbo, Xiaoxi Li, Jing Liu, Carolyn Rowinski, et al. 2017. "Determination of Receptor Occupancy in the Presence of Mass Dose: [11C]GSK189254 PET Imaging of Histamine H3 Receptor Occupancy by PF-03654746." *Journal of Cerebral Blood Flow & Metabolism* 37 (3): 1095–1107. https://doi.org/10.1177/0271678X16650697.

Gallezot, Jean-Dominique, David Weinzimmer, Nabeel Nabulsi, Shu-Fei Lin, Krista Fowles, Christine Sandiego, Timothy J. McCarthy, R. Paul Maguire, Richard E. Carson, and Yu-Shin Ding. 2011. "Evaluation of [11C]MRB for Assessment of Occupancy of Norepinephrine Transporters: Studies with Atomoxetine in Non-Human Primates." *NeuroImage* 56 (1): 268–79. https://doi.org/10.1016/j.neuroimage.2010.09.040.

Hillmer, A. T., I. Esterlis, J. D. Gallezot, F. Bois, M. Q. Zheng, N. Nabulsi, S. F. Lin, et al. 2016. "Imaging of Cerebral A4β2* Nicotinic Acetylcholine Receptors with (−)-[18F]Flubatine PET: Implementation of Bolus plus Constant Infusion and Sensitivity to Acetylcholine in Human Brain." *NeuroImage* 141 (November): 71–80. https://doi.org/10.1016/j.neuroimage.2016.07.026.

Jaworska, Natalia, Sylvia M. L. Cox, Maria Tippler, Natalie Castellanos-Ryan, Chawki Benkelfat, Sophie Parent, Alain Dagher, et al. 2020. "Extra-Striatal D2/3 Receptor Availability in Youth at Risk for Addiction." *Neuropsychopharmacology* 45 (9): 1498–1505. https://doi.org/10.1038/s41386-020-0662-7.

Kaller, Simon, Michael Rullmann, Marianne Patt, Georg-Alexander Becker, Julia Luthardt, Johanna Girbardt, Philipp M. Meyer, et al. 2017. "Test–Retest Measurements of Dopamine D1-Type Receptors Using Simultaneous PET/MRI Imaging." *European Journal of Nuclear Medicine and Molecular Imaging* 44 (6): 1025–32. https://doi.org/10.1007/s00259-017-3645-0.

Kantonen, Tatu, Tomi Karjalainen, Janne Isojärvi, Pirjo Nuutila, Jouni Tuisku, Juha Rinne, Jarmo Hietala, et al. 2020. "Interindividual Variability and Lateralization of μ-Opioid Receptors in the Human Brain." *NeuroImage* 217 (August): 116922. https://doi.org/10.1016/j.neuroimage.2020.116922.

Laurikainen, Heikki, Lauri Tuominen, Maria Tikka, Harri Merisaari, Reetta-Liina Armio, Elina Sormunen, Faith Borgan, et al. 2019. "Sex Difference in Brain CB1 Receptor Availability in Man." *NeuroImage* 184 (January): 834–42. https://doi.org/10.1016/j.neuroimage.2018.10.013.

Markello, Ross D., Justine Y. Hansen, Zhen-Qi Liu, Vincent Bazinet, Golia Shafiei, Laura E. Suárez, Nadia Blostein, et al. 2022. "Neuromaps: Structural and Functional Interpretation of Brain Maps." *Nature Methods*, October, 1–8. https://doi.org/10.1038/s41592-022-01625-w.

Naganawa, Mika, Nabeel Nabulsi, Shannan Henry, David Matuskey, Shu-Fei Lin, Lawrence Slieker, Adam J. Schwarz, et al. 2021. "First-in-Human Assessment of ^{11} C-LSN3172176, an M1 Muscarinic Acetylcholine Receptor PET Radiotracer." *Journal of Nuclear Medicine* 62 (4): 553–60. https://doi.org/10.2967/jnumed.120.246967.

Normandin, Marc D, Ming-Qiang Zheng, Kuo-Shyan Lin, N Scott Mason, Shu-Fei Lin, Jim Ropchan, David Labaree, et al. 2015. "Imaging the Cannabinoid CB1 Receptor in Humans with [11C] OMAR: Assessment of Kinetic Analysis Methods, Test–Retest Reproducibility, and Gender Differences." *Journal of Cerebral Blood Flow & Metabolism* 35 (8): 1313–22. https://doi.org/10.1038/jcbfm.2015.46.

Radhakrishnan, Rajiv, Nabeel Nabulsi, Edward Gaiser, Jean-Dominique Gallezot, Shannan Henry, Beata Planeta, Shu-fei Lin, et al. 2018. "Age-Related Change in 5-HT6 Receptor Availability in Healthy Male Volunteers Measured with 11C-GSK215083 PET." *Journal of Nuclear Medicine* 59 (9): 1445–50. https://doi.org/10.2967/jnumed.117.206516.

Sandiego, Christine M, Jean-Dominique Gallezot, Keunpoong Lim, Jim Ropchan, Shu-fei Lin, Hong Gao, Evan D Morris, and Kelly P Cosgrove. 2015. “Reference Region Modeling Approaches for Amphetamine Challenge Studies with [11C]FLB 457 and PET.” *Journal of Cerebral Blood Flow & Metabolism* 35 (4): 623–29. https://doi.org/10.1038/jcbfm.2014.237.

Sasaki, Takeshi, Hiroshi Ito, Yasuyuki Kimura, Ryosuke Arakawa, Harumasa Takano, Chie Seki, Fumitoshi Kodaka, et al. 2012. “Quantification of Dopamine Transporter in Human Brain Using PET with 18F-FE-PE2I.” *Journal of Nuclear Medicine: Official Publication, Society of Nuclear Medicine* 53 (7): 1065–73. https://doi.org/10.2967/jnumed.111.101626.

Satterthwaite, Theodore D., Russell T. Shinohara, Daniel H. Wolf, Ryan D. Hopson, Mark A. Elliott, Simon N. Vandekar, Kosha Ruparel, et al. 2014. “Impact of Puberty on the Evolution of Cerebral Perfusion during Adolescence.” *Proceedings of the National Academy of Sciences* 111 (23): 8643–48. https://doi.org/10.1073/pnas.1400178111.

Smith, C. T., L. C. Dang, J. W. Buckholtz, A. M. Tetreault, R. L. Cowan, R. M. Kessler, and D. H. Zald. 2017. “The Impact of Common Dopamine D2 Receptor Gene Polymorphisms on D2/3 Receptor Availability: C957T as a Key Determinant in Putamen and Ventral Striatum.” *Translational Psychiatry* 7 (4): e1091–e1091. https://doi.org/10.1038/tp.2017.45.

Subset Selection in Regression. 2002. Chapman and Hall/CRC. https://doi.org/10.1201/9781420035933.

Turtonen, Otto, Aino Saarinen, Lauri Nummenmaa, Lauri Tuominen, Maria Tikka, Reetta-Liina Armio, Airi Hautamäki, et al. 2021. “Adult Attachment System Links With Brain Mu Opioid Receptor Availability In Vivo.” *Biological Psychiatry: Cognitive Neuroscience and Neuroimaging* 6 (3): 360–69. https://doi.org/10.1016/j.bpsc.2020.10.013.

Weisberg, Sanford. 2014. *Applied Linear Regression*. John Wiley & Sons, Inc.

Woo, Choong-Wan, Liane Schmidt, Anjali Krishnan, Marieke Jepma, Mathieu Roy, Martin A. Lindquist, Lauren Y. Atlas, and Tor D. Wager. 2017. “Quantifying Cerebral Contributions to Pain beyond Nociception.” *Nature Communications* 8 (1): 14211. https://doi.org/10.1038/ncomms14211.

Yarkoni, Tal, and Jacob Westfall. 2017. “Choosing Prediction Over Explanation in Psychology: Lessons From Machine Learning.” *Perspectives on Psychological Science* 12 (6): 1100–1122. https://doi.org/10.1177/1745691617693393.